A Comprehensive Framework for Visualization of Natural and Anthropogenic Radioactivity for Applications in Environmental Monitoring

Naomi Park

Under the direction of
Dr. Haruko Murakami Wainwright
Professor of Nuclear Science and Civil and Environmental Engineering
Massachusetts Institute of Technology

Dr. Livia Fernandes Barros
Post Doctoral Associate
Massachusetts Institute of Technology

Research Science Institute
August 1, 2023

Abstract

Environmental pollution is a large challenge, causing irrevocable harm to the natural environment and human health. Radioactivity, a less-discussed aspect of environmental contamination, exists in two forms: natural, originating from the earth's formation, and anthropogenic, linked to human activities like nuclear power generation. The harms associated with radioactivity arise from its ionizing properties. Assessments and mitigation are, however, often complicated due to its ubiquity and overall spatial heterogeneity. Risk communication, in particular, requires to address background natural levels which vary across the world. As such, this research aims to tackle this challenge by developing a framework to effectively visualize and analyze both natural and anthropogenic radioactivity, based on latest python-based geospatial tools and machine learning approaches. We tested the framework in three locations: Camburi Beach, Brazil (naturally higher radioactivity), Chariot, Alaska (anthropogenic radioactivity from tracer experiments), and the Charles River, MA (unanalyzed for natural radioactivity). We demonstrated the whole workflow from sample collection to data visualization at 10 sampled locations along the Charles River. The two-part framework of interactive mapping and spatial interpolation, was then applied to capture each site's radioactivity distribution and heterogeneity. Lastly, A global map was created to analyze worldwide radioactivity distributions, highlighting Camburi Beach as having the highest absorbed gamma dose rate and variance among the three sites. In contrast, the anthropogenic contamination in Chariot, Alaska is nine orders of magnitude lower than other sites' natural radioactivity background, offering local communities perspective and assurance.

Summary

Environmental pollution poses severe risks to nature and human health, with radioactivity being a significant yet under-discussed contributor. Radioactivity, found naturally and also originating from human activities like mining and nuclear power, is difficult to mitigate due to its widespread and diverse distribution. Despite advancements in data science for pollution monitoring, effectively visualizing this data remains a challenge. Our research addresses this by creating a framework to visualize radioactivity, testing it at three sites: Camburi Beach, Brazil (high natural radioactivity), Chariot, Alaska (anthropogenic radioactivity), and the Charles River, MA (untested for radioactivity). This framework, involving interactive mapping and spatial distribution modeling, was applied to each site. A global map was also produced, highlighting the variations in radioactivity levels across the sites, with Camburi Beach having the highest dose rate and Chariot having the lowest.

1 Introduction

Environmental contamination is one of the most pressing challenges of our time as it causes irrevocable harm to not only ecosystems and the natural environment, but also human health [1]. Pollution is far reaching from air to water and encompasses a broad spectrum of substances such as heavy metals, organic compounds, pesticides, and plastics among others [2]. A less-discussed aspect of environmental contamination is radioactivity.

Radioactivity is a phenomenon by which an atom with an unstable nucleus spontaneously emits ionizing radiation to achieve stability [3]. Radioactivity broadly exists in two forms: natural and anthropogenic. Natural radioactivity is everywhere and has been present since the formation of the earth, found in elements like uranium, thorium, and potassium [4]. On the other hand, human activities such as nuclear power generation and production of nuclear weaponry have contributed to the creation of anthropogenic radioactive materials [5]. The effects of radioactivity are complex and multifaceted, rooted in its ionizing properties that have the potential to damage DNA, causing both single- and double-strand breaks [6]. Prolonged exposure to ionizing radiation may contribute to cell mutations and elevate the risk of cancer [6]. However, it's important to note that organisms possess DNA repair mechanisms, and the relationship between low-level radiation and health effects remains a subject of ongoing research and debate [7].

Radioactive contamination is generally associated with infamous sites like Fukushima or Chernobyl. However, at more than a hundred locations in the United States today, there are radiological contamination sites associated with nuclear weapons proliferation and nuclear energy. For example, Chariot, Alaska was identified as a potential location to use a series of nuclear explosions to excavate a harbor. Although the project was canceled, radioactive tracer experiments were performed which released anthropogenic radionuclides to observe radionuclide transport in the environment. Due to the lack of monitoring and ineffective communication, there are ongoing public concerns surrounding potential exposure to radioactivity in nearby areas [8].

At the same time, there are naturally occurring radionuclides in soil such as K-40, uranium and thorium decay series, often associated with specific geological environments such as granitic rocks or fine/organic-rich sediments. There is an increasing awareness of such naturally radioactive elements. For example, recent literature, has linked indoor radon exposure to lung cancer, [9] and although there are mitigation strategies such as radon testing and ventilation in houses, it is not a widely recognized nor adopted practice [10].

The challenge for monitoring radioactivity is three fold. Firstly, sample collection and analyses are usually expensive and labor intensive. Secondly, government-led environmental monitoring often fails to address community concerns. Thirdly, the non-uniform distribution of radioactivity, influenced by factors such as geology and hydrology, adds complexity to monitoring efforts [11].

Advances in data science are significantly improving environmental pollution monitoring. Through tools like Google Earth Engine, researchers can now easily access and analyze vast geospatial data to better track and monitor pollution [12]. Machine learning algorithms have also played a significant role, optimizing interpolation, mapping, and sensor placement. [13]. Despite these innovations, challenges remain in seamlessly integrating mapping and creating effective data visualizations within current machine learning frameworks.

As such, the goal of this research is to develop a comprehensive data science framework from point data to mapping, effective data visualization and spatial interpolation for radioactivity. This framework aims to enable a systematic evaluation and understanding of global and site-specific distributions of anthropogenic and natural radioactivity. It aims to contribute to a more precise and nuanced understanding of the local and global radioactivity landscape and its potential implications for humans and the environment.

2 Methodology

The research follows a workflow that encompasses three key phases: (1) the collection of sediment samples from different geographical points; (2) the utilization of gamma spectrom-

etry analyses to measure radioactivity within these samples; and (3) the implementation of a two park framework, comprising interactive mapping and Gaussian Processes for spatial interpolation.

The framework's efficacy will be demonstrated using three locations: Camburi Beach in Espírito Santo, Brazil (natural higher background of radioactivity), Chariot, Alaska (anthropogenic due to radioactive tracer experiments), and the Charles River in Cambridge, MA, a local site lacking current radioactivity analyses. The Charles River will serve as a comprehensive example, illustrating the entire workflow from data collection to visualization.

2.1 Gamma Spectrometry

Gamma spectrometry was utilized to identify and quantify the concentration of naturally occurring radioactive isotopes based on the gamma-rays emitted during radioactive decay. This technique is particularly useful in assessing natural radioactivity for several reasons. Firstly, it allows for the measurement of multiple radionuclides simultaneously without the need for tedious processes such as radiochemical separation [14]. Secondly, it is a non-destructive method that preserves the integrity of the sample enabling further analysis if required. Thirdly, due to its high sensitivity, it is capable of detecting and quantifying natural radioactivity, even when present at low levels [15].

Although many naturally occurring elements have radioactive isotopes, only specific ones, including potassium, and isotopes from the uranium and thorium decay series produce gamma rays of sufficient energy and intensity to be measured via gamma spectrometry. This is mainly due to their abundance in nature [16]. However, in order to accurately measure the radioactive isotopes of uranium and thorium, samples typically need to be set aside for approximately a month to achieve secular equilibrium. Given these temporal constraints, only Potassium-40 (K-40) concentrations were analyzed. The measurements were conducted using a high-purity germanium (HPGe) detector.

2.1.1 Soil Sample Collection

Ten points were sampled along the Charles River with a focus on comparing proximity to the water, opposing banks, and differences among parks and beaches to examine several factors. The following enumerates the justifications of focusing on these variables:

1. **Water flow and sediment transportation:** Water can be a medium of transport for naturally radioactive elements found in sediment [17]. Furthermore, a river's flow could lead to differences in depositional behavior on opposing banks. Typically, the inner bend of a river has a slower flow, leading to more sediment deposition, while the outer bend experiences faster flows, causing more erosion [18]. These dynamics could potentially contribute to differing levels of natural radioactivity on opposing banks as well as in soil that is closer to the water.

2. **Geological differences:** The geological makeup of different riverbanks and parks can cause differences in natural radioactivity levels. Some rock types, like clays, usually contain higher concentrations of radioactive elements [19].

(a) (b)

Figure 1: (a) Map of Charles River highlighting 10 sample collection points (b) Soil sample in 250ml polyethylene vial in HPGe detector

At each of the specified locations summarized in Figure 1a, roughly 0.5kg of soil was collected and sealed into a sterile, labeled, zip-lock plastic bag to avoid any potential contamination. The locations were targeted to represent soil native to the Charles River. The focus on native soil allows for an accurate reflection and analysis of the geological conditions that are characteristic to this region.

2.1.2 Preparation and Analysis of Soil Samples

Once the soil samples were collected from the 10 sites, the subsequent phase involved preparing the samples for gamma spectrometry analyses. Each 250ml polyethylene vial was first weighed in its empty state. The soil at each respective location was then transferred to the corresponding vial, each filled to capacity. The vials were then weighed again to obtain the gross weight (soil + vial) and the net weight (soil only). For the radioactivity analysis, a filled vial was placed in a High Purity Germanium (HPGe) detector for a 24-hour duration (see Figure 1b).

2.2 Part 1: Interactive Mapping

The radioactivity data of soil and sand samples collected via gamma spectrometry analyses, coupled with the geographical coordinates of the sampling locations, were organized into a data frame. These parameters act as the primary input for the first component of the framework - effective visualization utilizing ipyleaflet for interactive mapping. An interactive program is implemented as it is better suited to achieve the goals of this project: effective communication and visualization of data to the public.

The "plotmap" function was developed to produce these visualizations. This function starts by normalizing the radioactivity measurements collected between 0 and 1. It then associates colors to the data depending on their scaled values, producing a gradient scheme from dark blue to dark red. Subsequently, an interactive map is generated with circle markers positioned at the locations defined by the latitude and longitude coordinates. The colors of

these markers follow the previously designated color associated with the respective radioactivity measurements. For each marker, a popup message reveals the precise coordinates and the absorbed dose rate in nGy/hr at each respective location. Finally, to interpret the colors, a horizontal color bar is embedded into the map, using the same color gradient as the markers.

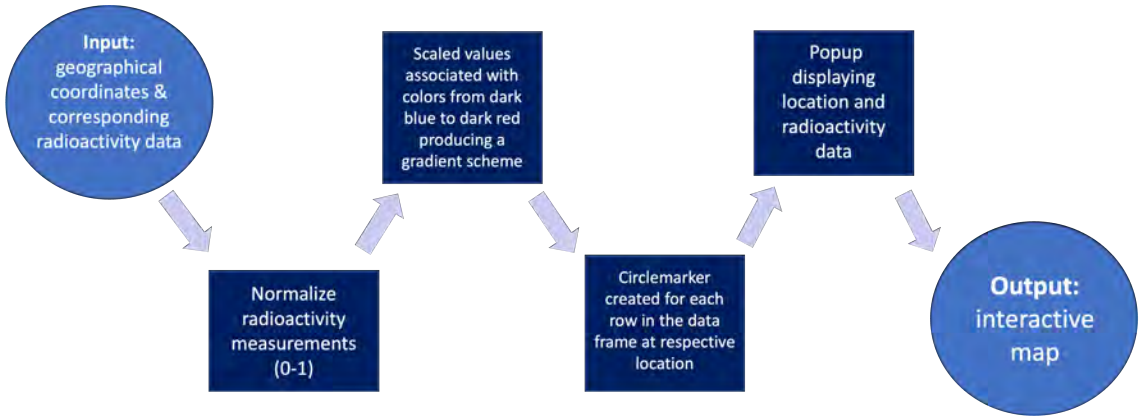

Figure 2: Flowchart of "plotmap" function components

2.3 Part 2: Spatial Interpolation using Gaussian Process

Although interactive mapping is effective in visualizing contaminant concentrations at specific points, it is unable to serve other functions, such as estimating radioactivity concentrations at untested points. To address this limitation, the second component of the framework applies a Gaussian Process Regression to capture the spatial heterogeneity and perform interpolation on radioactivity data at each of the sites. The Gaussian Process was chosen over existing supervised learning models because it provides a measure of uncertainty along with its predictions, as shown in Figure 3 [20]. This is a particularly useful feature as the data being analyzed is limited.

To apply the Gaussian Process, The geographic coordinates (latitude and longitude) are transformed to Universal Transverse Mercator (UTM) coordinates. Transformation to UTM is crucial as unlike angular coordinate systems like latitude and longitude, UTM provides a constant distance relationship on a map, streamlining subsequent spatial computations.

Next, we define a prediction grid for the region of interest by establishing a grid based

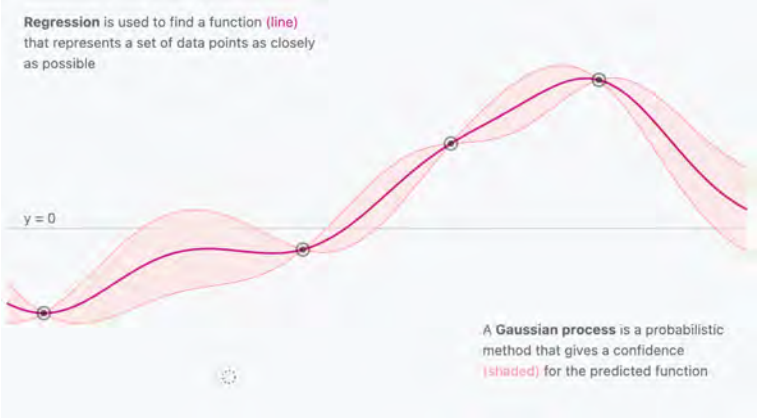

Figure 3: Visual representation of GPR [21]

on the range of UTM coordinates. The training data consists of the transformed UTM coordinates and the absorbed dose rate of radioactivity at each point. However, the absorbed dose rates can span a broad range of values that may follow a skewed distribution. This can lead to potential challenges in the model's learning process. Therefore, the logarithm of the absorbed dose rate is taken to normalize these values.

The Gaussian Process model is implemented using various functions from the "gpcam" library, a python-based framework for approximation, optimization, and autonomous experimentation [22]. The model uses a Radial Basis Function (Gaussian) kernel.

After the model is trained with the inputted data, a prediction on the entire grid of points defined earlier is made, simulating estimations of radioactivity levels over a larger area. This essentially estimates potential radioactivity levels at locations where no actual measurements were obtained which is particularly useful in environmental monitoring, where it's not always feasible to take measurements at every location.

These predictions are then visualized in three ways. The first visualization is a scatter plot of the original samples in the UTM space, color-coded by their absorbed dose rate values. The second visualization overlays the Gaussian Process' predicted radiation dosage field onto the scatter plot of the original samples. The final visualization shows the variance in the predictions from the Gaussian Process.

3 Results & Discussions

3.1 Camburi Beach

The absorbed dose rates (nGy/h) of radioactivity found at the 11 locations along Camburi beach were plotted (Figure 4). Upon examining the data, locations 2 and 5 were observed to have significantly higher dose rates of 758 nGy/h and 827 nGy/h, respectively. These values are notably higher than other recorded values, which ranged from 12 to 122 nGy/h, distinguishing them as outliers within the spatial distribution of radioactivity (see Table 1). The average dose rate was calculated at 190.82 nGy/h with a standard deviation (SD) of 300.24 nGy/h.

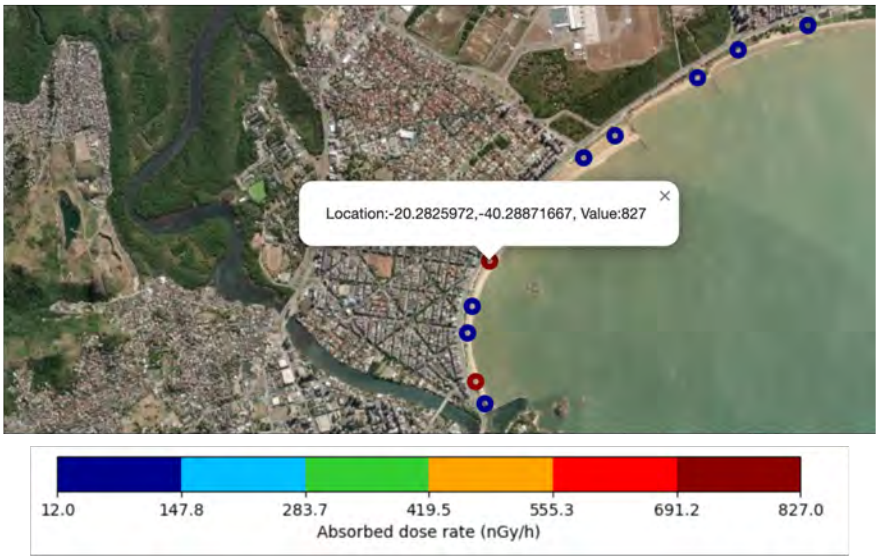

Figure 4: Interactive map of Camburi Beach natural radioactivity data

Spatial interpolation and confidence interval analyses were effectively conducted using Gaussian Process (GP) tools, as displayed in Figure 5. The overlay of the GP's radiation dosage field prediction correlates with the identified anomalies at locations 2 and 5, signifying higher dose rates in areas adjacent to the known concentrations at the sampled points. This distribution is in line with previous studies of natural radioactivity at Camburi beach [16].

Finally, the GP's prediction field overlaid onto the geographical boundaries of Camburi Beach allows for a visual representation of the spatial distribution of radiation, highlighting

its immense heterogeneity even within a localized site (see Figure 6).

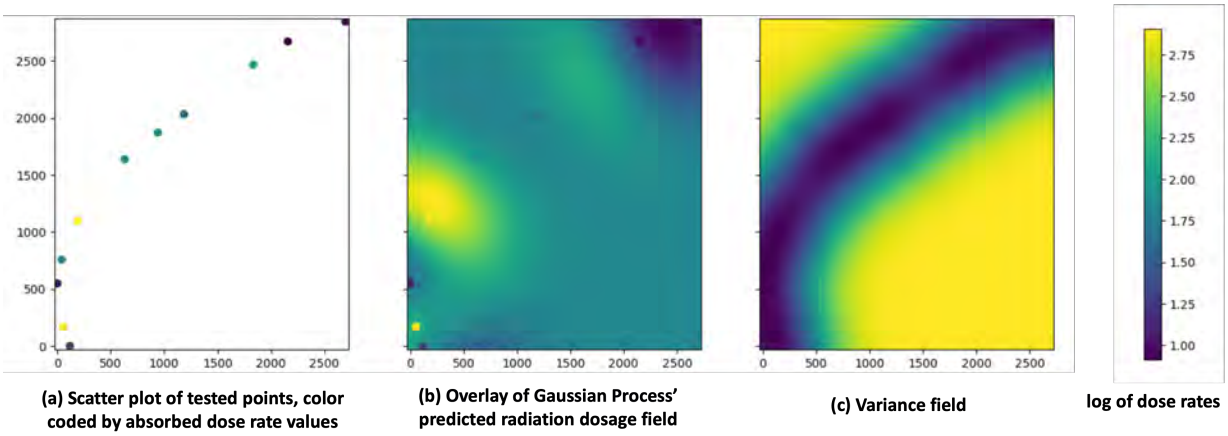

Figure 5: Visualization of GP predictions and uncertainty on Camburi Beach radioactivity data

Figure 6: GP prediction of the radiation dosage field overlaid onto the geographical boundaries of Camburi Beach

3.2 Charles River

Following gamma spectrometry analyses of all ten soil samples from the Charles River, the activity concentration of K-40 (Bq/kg) and absorbed dose rate (nGy/h) was successfully determined. The peak height of K-40 at 1460 keV was first identified across all samples. To

calculate activity concentration, the net peak area of the sample, the net peak area of the background K-40, and the sample's activity in Bq were utilized. The activity concentration was multiplied by the dose factor of K-40 (0.0417) [16], resulting in the determination of the absorbed dose rate (see Table 2).

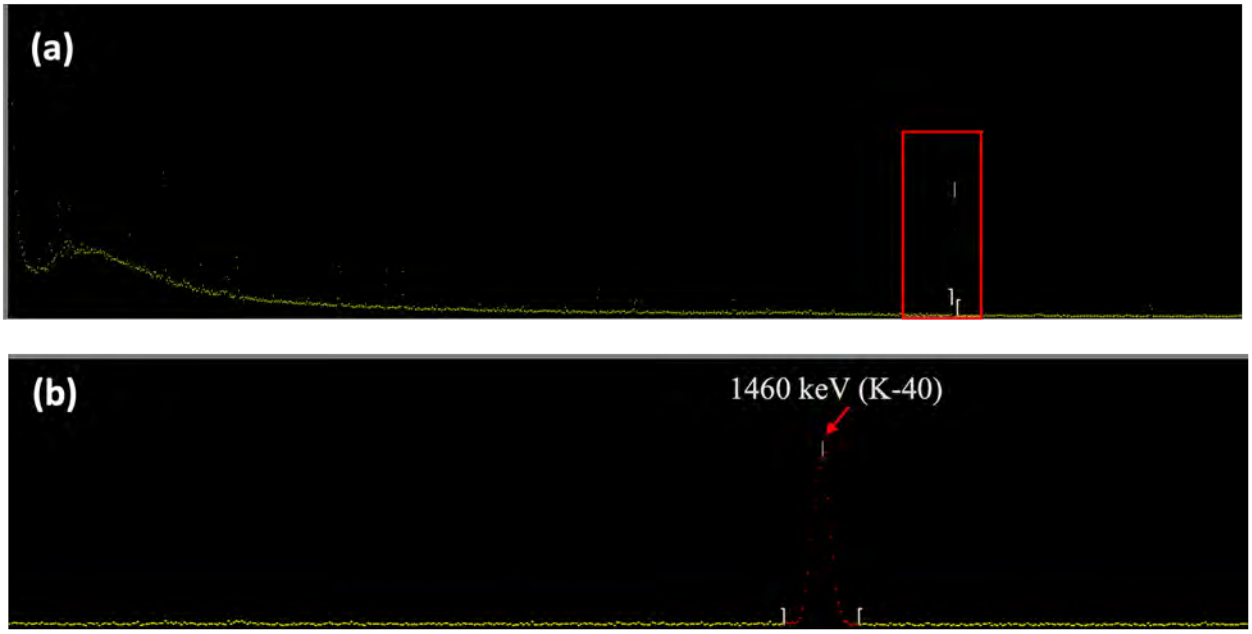

Figure 7: (a) Full gamma spectrum obtained of soil sample Herter 3. (b) Magnified view of spectrum highlighting K-40 peak at 1460 keV

Given that no analyses have currently been done on natural radioactivity in soil along the Charles River, the collected gamma spectrometry data with the integration of the framework highlights some key results. The data reveals a relatively consistent distribution of radioactivity. The dose rate associated with K-40 fluctuated between 13.01-26.08 nGy/h, averaging at 18.61 nGy/h. The SD of 5.37 nGy/h suggests that considerable heterogeneity is not present in this particular region. However, it's crucial to note that this doesn't indicate a uniform data distribution either, thus again underscoring the inherent heterogeneity of radioactivity, even within localized regions.

When analyzing proximity to the river as a potential factor of radioactivity, it can be seen that in each case where river proximity was analyzed, the sample closer to the river exhibited a higher activity concentration and thus dose rate from K-40. This pattern could

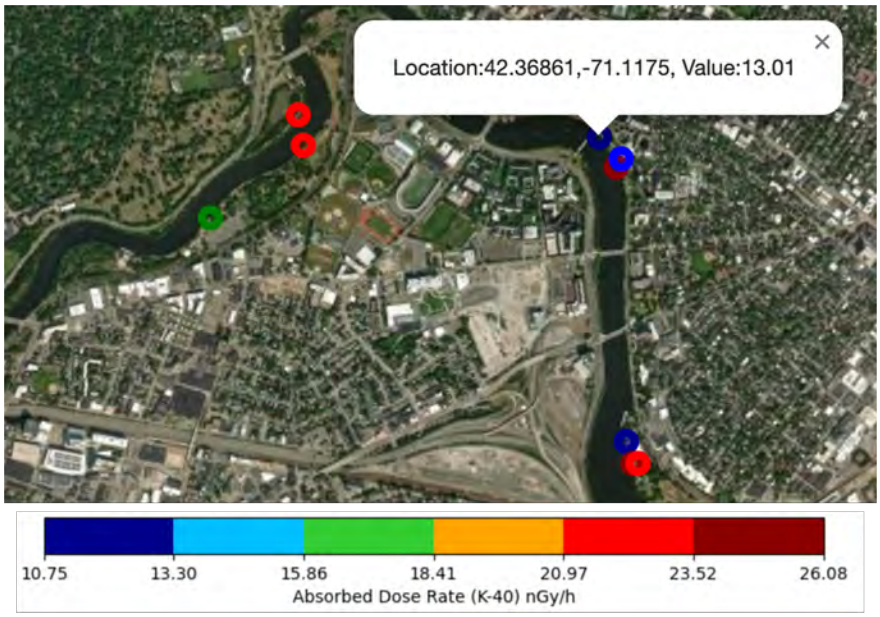

Figure 8: Interactive map of Charles River natural radioactivity data

potentially be attributed to the prevalence of fine-grained sediments such as clay [23] and silt near the river. These sediments often have higher concentrations of K-40 due to various factors, such as weathering, increased surface area, and sediment transportation. The flow of the river facilitates the transport and deposition of these weathered materials, causing areas closer to the riverbed to accumulate these sediments of higher K-40 concentrations.

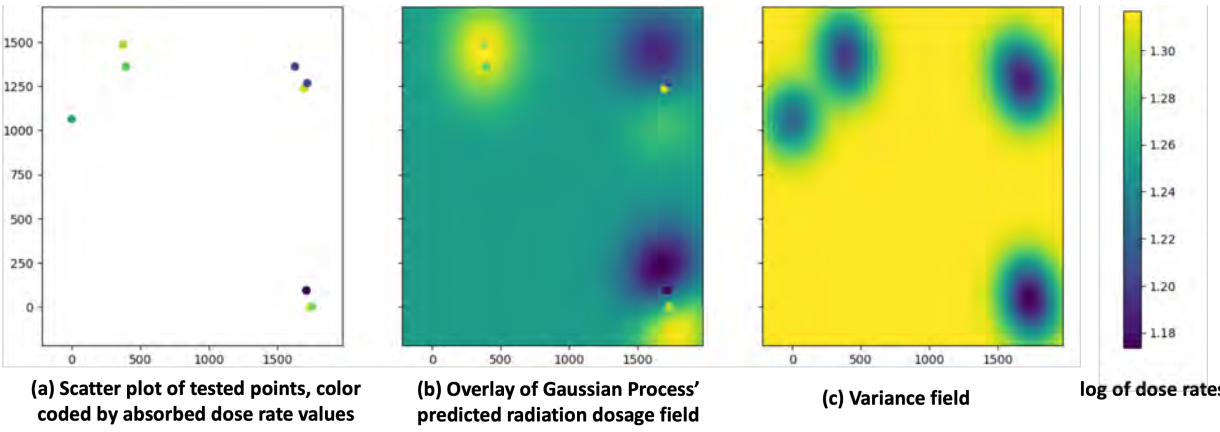

Figure 9: Visualization of GP predictions and uncertainty on Charles River natural radioactivity data

3.3 Chariot, Alaska

Historically, Project Chariot in Chariot, Alaska led to public concern regarding potential radioactive contamination due to the use of radioactive tracers such as Cesium-137 in localized test plots. This unease was primarily driven by insufficient and ineffective communication to the public about the real concentrations of the tracers [24].

The application of the framework as well as conversion of the reported Cesium-137 concentrations from (pCi/g) to (nGy/h) (see Table 3) as per the methods outlined by Shibata et al. [25] provides a clear understanding of the extent of harm that could be caused by these tracer experiments (Figure 10). It indicates that the radiation levels the local community was exposed are significantly lower than typical natural background radiation, which generally measures in the hundreds of nGy/h [26]. Specifically, the exposure levels averaged at 1.62 E-8 nGy/h , with a SD of 1.14 E-8 nGy/h, demonstrating a difference spanning multiple orders of magnitude compared to average natural radiation.

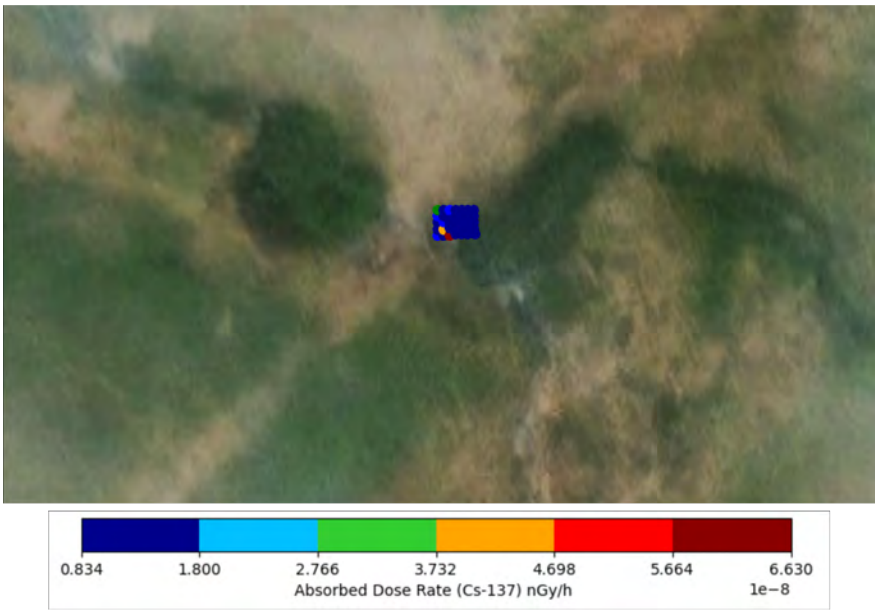

Figure 10: Interactive map of anthropogenic radioactivity data in test plot in Chariot, Alaska

The demonstration of the framework's efficacy on radioactivity data from Project Chariot emphasizes its versatility and applicability beyond assessments of natural radioactivity, ex-

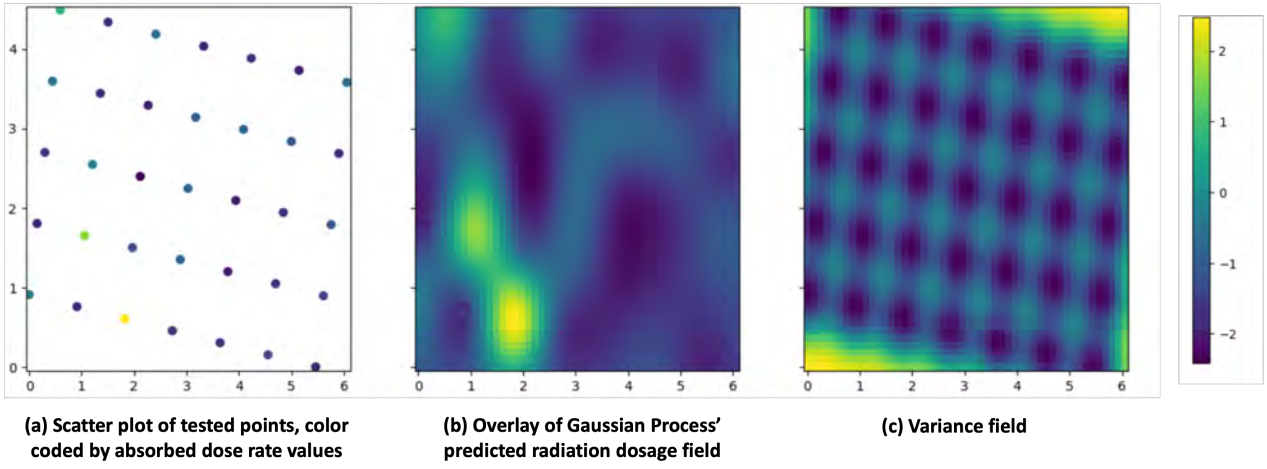

Figure 11: Visualization of GP predictions and uncertainty on Chariot anthropogenic radiaoctivity data

tending to visualization of anthropogenic radioactive pollutants, which tend to be the source of more public concern.

3.4 Global Mapping

Utilizing the three locations analyzed in this research, a preliminary, interactive global map is created and visualized (see Figure 12):

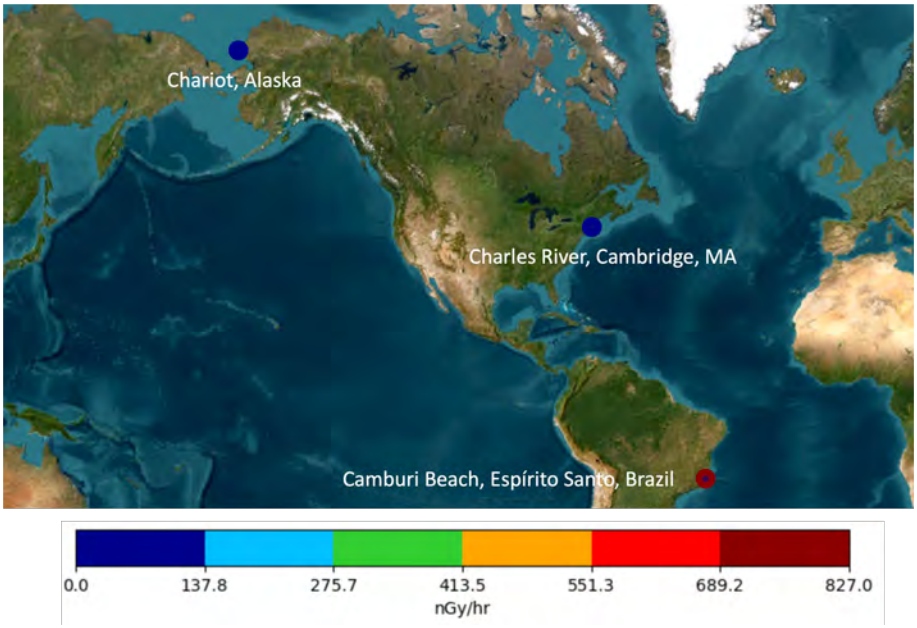

Figure 12: Global interactive map of three sites (Charles River, Camburi Beach, Chariot)

Upon reviewing the map, it is apparent that of the three sites examined, Camburi Beach has the highest absorbed gamma dose rate, primarily attributed to the two outliers identified in Figure 13. The map also emphasizes that the anthropogenic contamination in Chariot is negligible when compared to levels of natural radioactivity found globally. This comparison provides valuable perspective for local communities concerned about potential radioactive contamination, helping to contextualize its actual impact.

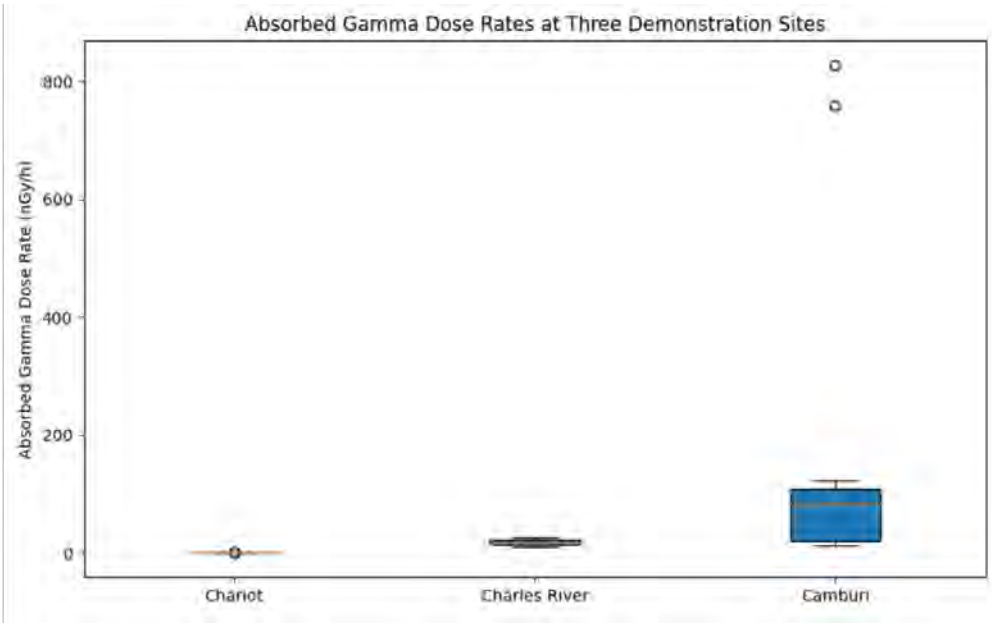

Figure 13: Boxplot of absorbed dose rate values at each site highlighting outliers and distribution of site-specific radioactivity

When the natural radioactivity sites, Charles River and Camburi Beach, are compared, there is a marked difference in their heterogeneity. In particular, the standard deviation of data from Camburi Beach is significantly higher, with an SD = 300.24 nGy/h, compared to Charles River's SD = 5.37 nGy/h. It is worth noting that due to time constraints, the absorbed dose rate for Charles River was calculated solely based on the activity concentration of K-40. Despite this limitation, these derived values are still comparable and provide crucial insights into a site's natural radioactivity and comparison of other features like distribution and heterogeneity to other sites around the world.

4 Conclusions & Future Work

Efforts to achieve a comprehensive understanding of global radioactivity distributions is an existing effort entitled "D-shuttle" pioneered by high school students from Japan, France, Poland, and Belarus who assessed radiation levels in the aftermath of the Fukushima Daiichi nuclear power disaster [27]. While their work contributed to a broader understanding of radiation levels in varied geographical contexts, it was primarily focused on measurement and comparison of individual external doses in specific locations. There were shortcomings in terms of effectively visualizing the collected data. As such, this framework aims to build upon their initial aims by not only quantifying radiation levels, but also incorporating techniques of spatial interpolation and data visualization.

The goals of this research were achieved as a framework was succesfully created that serves three main purposes:

First, it provides a macroscopic perspective on the global radioactivity distribution. This global overview is fundamental in comprehending the varying levels of natural and anthropogenic radioactivity worldwide. It lends context and perspective to concerns regarding anthropogenic radioactivity and seeks to address current limitations in environmental monitoring: data visualization and communication.

Second, the map's interactive features allow zooming in on specific sites for a more localized analysis on radioactivity distributions and concentrations. This site-specific perspective is critical for understanding patterns, variances, and heterogeneity in a regional context.

Third, the use of Gaussian Processes for spatial interpolation allows us to model and estimate radioactivity levels at unmeasured locations. By leveraging the spatial correlations between measured and unmeasured points, this technique fills in gaps and provides a more comprehensive understanding of the spread and scope of radioactivity.

In light of escalating concerns about the potential harms of natural and anthropogenic radioactivity, future work will consist of acquiring a more expansive and diverse range of data from across the globe, thereby enhancing the nuanced understanding of the spatial

heterogeneity and distribution of radioactivity.

Moreover, the utility of the framework developed in this project extends beyond addressing the issue of radioactivity. Given its adaptability and applicability, another crucial aim of the future will be to leverage this framework in the monitoring and mitigation of other hazardous forms of environmental pollution.

5 Acknowledgments

I would like to thank Professor Haruko Murakami Wainwright and Dr. Livia Fernandes Barros for their invaluable support and guidance throughout the research process. I would also like to thank my tutor Agnes Robang and the Center for Excellence in Education and the Massachusetts Institute of Technology for sponsoring and hosting the 40th Research Science Institute.

References

[1] Health consequences of air pollution on populations. Available at https://www.who.int/news/item/15-11-2019-what-are-health-consequences-of-air-pollution-on-populations#:~:text=Exposure%20to%20high%20levels%20of,people%20who%20are%20already%20ill (2023/07/06).

[2] N. Geographic. Pollution, 2023. URL https://education.nationalgeographic.org/resource/pollution/. Accessed: 29 July 2023.

[3] C. Grupen, M. Rodgers, C. Grupen, et al. *What are radioactivity and radiation?* Springer, 2016.

[4] Naturally occurring radioactive elements. Available at https://www.healthvermont.gov/environment/radiological/radioactive-elements (2023/07/06).

[5] Man made sources. Available at https://www.nrc.gov/about-nrc/radiation/around-us/sources/man-made-sources.html (2023/07/09).

[6] A. Goodarzi, A. Anikin, and D. Pearson. Environmental sources of ionizing radiation and their health consequences. In *Genome stability*, pp. 569–581. Elsevier, 2016.

[7] T. Neumaier, J. Swenson, C. Pham, et al. Evidence for formation of dna repair centers and dose-response nonlinearity in human cells. *Proceedings of the National Academy of Sciences*, 109(2):pp. 443–448, 2012.

[8] Chariot, alaska, site. Available at https://www.energy.gov/lm/chariot-alaska-site (2023/07/09).

[9] J. M. Samet. Radon and lung cancer. *JNCI: Journal of the National Cancer Institute*, 81(10):pp. 745–758, 1989.

[10] R. Hoffmann. Radon contamination of residential structures: mitigation strategies and 'the weather effect. In *Proceedings of The International Radon Conference, USA, Colorado, VII-1–VII-8*. Citeseer, 1993.

[11] N. Ahmad, M. S. Jaafar, M. Bakhash, et al. An overview on measurements of natural radioactivity in malaysia. *Journal of radiation research and applied sciences*, 8(1):pp. 136–141, 2015.

[12] Q. Zhao, L. Yu, X. Li, et al. Progress and trends in the application of google earth and google earth engine. *Remote Sensing*, 13(18):p. 3778, 2021.

[13] M. Hino, E. Benami, and N. Brooks. Machine learning for environmental monitoring. *Nature Sustainability*, 1(10):pp. 583–588, 2018.

[14] Z. Zhou, H. Ren, L. Zhou, et al. Recent development on determination of low-level 90sr in environmental and biological samples: A review. *Molecules*, 28(1):p. 90, 2022.

[15] A. Murray, R. Marten, A. Johnston, et al. Analysis for naturally occuring radionuclides at environmental concentrations by gamma spectrometry. *Journal of Radioanalytical and Nuclear Chemistry*, 115(2):pp. 263–288, 1987.

[16] L. F. Barros and B. R. Pecequilo. The influence of environmental aspects in the variation of natural radioactivity levels in selected brazilian beach sand samples. *Erosion, Management Practices and Environmental Implications*, p. 73, 2014.

[17] A. El-Gamal, S. Nasr, and A. El-Taher. Study of the spatial distribution of natural radioactivity in the upper egypt nile river sediments. *Radiation measurements*, 42(3):pp. 457–465, 2007.

[18] V. A. Vanoni. River dynamics. *Advances in applied mechanics*, 15:pp. 1–87, 1975.

[19] Radiation exposure from medical exams and procedures, 2023. URL `https://hps.org/publicinformation/ate/q12844.html`. Accessed: 2023-07-23.

[20] An intuitive guide to gaussian processes, 2023. URL `https://towardsdatascience.com/an-intuitive-guide-to-gaussian-processes-ec2f0b45c71d`. Accessed: 2023-07-23.

[21] J. Li, C. Carroll, T. Vincent, et al. A visual exploration of gaussian processes. *Distill*, 2019. URL `https://distill.pub/2019/visual-exploration-gaussian-processes/`. Accessed: 2023-07-23.

[22] Gpcam: Global precipitation measurement, 2023. URL `https://gpcam.lbl.gov/`. Accessed: 2023-07-23.

[23] G. J. Levy and A. Bar-Tal. Alkali metals in soils. 2023.

[24] U. D. of Energy. Chariot, alaska site. `https://www.energy.gov/lm/chariot-alaska-site`, n.d. Accessed July 29, 2023.

[25] K. Saito, I. Tanihata, M. Fujiwara, et al. Detailed deposition density maps constructed by large-scale soil sampling for gamma-ray emitting radioactive nuclides from the fukushima dai-ichi nuclear power plant accident. *Journal of environmental radioactivity*, 139:pp. 308–319, 2015.

[26] Background radiation. `https://radwatch.berkeley.edu/background-radiation`, n.d. Accessed July 29, 2023.

[27] M. Prosser. How 200 japanese high school students became fukushima fallout scientists. `https://www.forbes.com/sites/prossermarc/2016/04/15/how-200-japanese-high-school-students-became-fukushima-fallout-scientists/?sh=7e4c92df2332`, 2016. Accessed July 29, 2023.

Appendix

A Geographical coordinates & radioactivity data for map visualizations

Location ID	Latitude	Longitude	Dose Rate (nGy/h)
1	-20.292469	-40.289125	27
2	-20.290961	-40.289766	758
3	-20.287569	-40.290388	15
4	-20.285686	-40.290066	83
5	-20.282597	-40.288716	827
6	-20.277597	-40.284672	95
7	-20.275411	-40.281763	91
8	-20.273902	-40.279477	56
9	-20.269816	-40.273405	122
10	-20.267902	-40.270369	12
11	-20.266191	-40.265272	13

Table 1: Summary of Camburi Beach natural radiaoctivity data (absorbed dose rate in nGy/h) with corresponding geographical coordinates of 11 tested points

Location ID	Latitude	Longitude	K-40 conc. (Bq/kg)	Dose Rate (nGy/h)
Herter 1	42.3656	-71.1372	431.22	17.98
Herter 2	42.3683	-71.1325	503.80	21.01
Herter 3	42.3694	-71.1328	552.88	23.06
Magazine 1A	42.3572	-71.1161	355.15	14.81
Magazine 1B	42.3572	-71.1161	257.75	10.75
Magazine 2A	42.3564	-71.1158	625.47	26.08
Magazine 2B	42.3564	-71.1156	518.73	21.63
Riverbend 1A	42.3675	-71.1167	585.37	24.41
Riverbend 1B	42.3678	-71.1164	320.31	13.36
Riverbend 2A	42.3686	-71.1175	312.04	13.01

Table 2: Summary of sampling locations, corresponding coordinates, calculated K-40 activitiy concentration (Bq/kg), and dose rates (nGy/h) along the Charles River. Locations ending with 'A' are close to the river while locations ending with 'B' are farther (10 ft out)

ID	**Latitude**	**Longitude**	**Dose Rate** ($\times 10^{-8}$) **(nGy/h)**
1	68.10665071	-165.7646995	1.15
2	68.10668341	-165.7647225	0.991
3	68.10667521	-165.7647223	1.56
4	68.10666701	-165.764722	1.69
5	68.10665881	-165.7647217	1.67
6	68.10665061	-165.7647215	1.15
7	68.10668331	-165.7647445	1.82
8	68.10667511	-165.7647442	0.991
9	68.10666691	-165.764744	0.834
10	68.1066587	-165.7647437	1.38
11	68.1066505	-165.7647434	6.63
12	68.10668321	-165.7647665	1.12
13	68.106675	-165.7647662	1.09
14	68.1066668	-165.7647659	2.08
15	68.10666721	-165.7646781	1.09
16	68.10665901	-165.7646778	1.12
17	68.10665081	-165.7646775	1.35
18	68.10668351	-165.7647006	1.15
19	68.10667531	-165.7647003	1.67
20	68.10666711	-165.7647	0.964
21	68.10665891	-165.7646998	0.964
22	68.1066586	-165.7647657	4.68
23	68.1066504	-165.7647654	1.07
24	68.1066831	-165.7647885	3.30
25	68.1066749	-165.7647882	1.92
26	68.1066667	-165.7647879	1.17
27	68.1066585	-165.7647876	1.01
28	68.1066503	-165.7647874	2.00
29	68.10668371	-165.7646566	1.77
30	68.10667551	-165.7646564	1.07
31	68.10666731	-165.7646561	1.48
32	68.10665911	-165.7646558	1.28
33	68.10665091	-165.7646555	1.02
34	68.10668361	-165.7646786	0.991
35	68.10667541	-165.7646783	1.51

Table 3: Summary of Project Chariot radioactivity data from anthropogenic Cs-137 tracers with corresponding geographical coordinates